

Rabi oscillations in a quantum dot-cavity system coupled to a non-zero temperature phonon bath

Jonas Larson¹ and Héctor Moya-Cessa²

¹ICFO-Institut de Ciències Fotòniques, E-08860 Castelldefels, Barcelona, Spain

²INAOE, Coordinación de Óptica, Apdo. Postal 51 y 216, 72000 Puebla, Pue., Mexico

(Dated: December 20, 2018)

We study a quantum dot strongly coupled to a single high-finesse optical microcavity mode. We use a rotating wave approximation method, commonly used in ion-laser interactions, to obtain an analytic solution of this problem beyond the Born-Markov approximation. The decay of Rabi oscillations because of the electron-phonon coupling are studied at arbitrary temperature and analytical expressions for the collapse and revival times are presented. Analysis without the rotating wave approximation are presented and new structures and phenomena of the Rabi oscillations occur in this regime either due to level crossings of the energy eigenvalues or because of equidistant eigenenergies.

PACS numbers: 73.21.La, 42.50.Pq, 03.67.Lx

I. INTRODUCTION

Semiconductor quantum dots (QD) have emerged as promising candidates for studying quantum optical phenomena [1]. In particular, cavity quantum electrodynamics (CQED) effects can be investigated using a single QD embedded inside a photonic nano-structure [2]. One of the most fundamental systems in CQED is an atom interacting with a quantized field [3], such a system has been an invaluable tool to understand quantum phenomena [4] as well as for considerations on its applications to realize quantum information [5]. Similar systems (in the sense of their treatment, applications, etc.) like trapped ions interacting with lasers [6] have shown to be an alternative to develop techniques for quantum information processing [7] and the study of fundamental effects [8]. Recent developments in semiconductor nano-technology have shown that excitons in QD constitute also an alternative two-level system for CQED effects [9]. Contrary to the atom-field interaction where dissipative effects can be fairly overlooked provided the coupling strength between atom and field is sufficiently large compared to the dissipation rate due to cavity losses, the physics of a quantum dot microcavity is enriched by the presence of electron-electron and electron-phonon interactions, indicating that decoherence due to phonons may imply fundamental limitations to quantum information processing on quantum dot CQED [10]. Here, we would like to analyze the effects of electron-phonon interactions on electron-hole-photon Rabi oscillations in cavity QED.

As in Ref. [11, 12], we will not apply the Born-Markov approximation [13], but we will use a different technique for solving this problem. In particular we will make use of techniques commonly applied in ion-laser interactions. It relies on the rotating wave approximation RWA, and within this approximation the Hamiltonian becomes diagonal with respect to the phonon subsystem, which is shown in sec. II. In the validity regime of the RWA, the decoherence effect on the inversion, due to the phonon bath, is analyzed in sec. III. Further approximations, valid in large parameter ranges, are introduced in order

to achieve analytical expressions for the collapse and revival times. The zero temperature situation has been investigated in [12], while here we study the effects due to zero as well as non-zero temperatures (causing the collapse of the revivals), as also how different phonon mode structures affect the decoherence. A different method to treat the non-zero temperature case was discussed in [14], where the collapse time is obtained numerically. The dynamics beyond the rotating wave approximation, studied here in sec. IV, possess several new phenomena which are numerically and analytically analyzed in terms of the eigenvalue spectrum. In particular, due to level crossings, the involved Rabi phases contain non-analytic behaviors resulting in *dislocation*-like properties in the "time-frequency" diagram. We also show and explain that for certain parameter values the collapse-revival pattern is lost, which is counterintuitive as the dot-cavity system is coupled to a set of Fock states all with different corresponding "energies".

II. THE MODEL

We assume a simple two-level model for the electronic degrees of freedom of the QD, consisting of the QD electronic ground state, $|g\rangle$, and the lowest energy electron-hole (exciton) state, $|e\rangle$, with the Hamiltonian [11] ($\hbar = 1$)

$$\hat{H} = \omega_{eg}\hat{\sigma}_{ee} + \omega\hat{a}^\dagger\hat{a} + g(\hat{a}^\dagger\hat{\sigma}_- + \hat{\sigma}_+\hat{a}) + \hat{\sigma}_{ee}\sum_k \lambda_k(\hat{b}_k^\dagger + \hat{b}_k) + \sum_k \omega_k \hat{b}_k^\dagger \hat{b}_k, \quad (1)$$

where $\hat{\sigma}_+ = |e\rangle\langle g|$, \hat{a} and \hat{b}_k are the annihilation operators for the cavity mode and the k th phonon mode, respectively. By transforming to a rotating frame, with frequency ω

$$\hat{\mathcal{H}} = \Delta\hat{\sigma}_{ee} + g(\hat{a}^\dagger\hat{\sigma}_- + \hat{\sigma}_+\hat{a}) + \hat{\sigma}_{ee}\sum_k \lambda_k(\hat{b}_k^\dagger + \hat{b}_k) + \sum_k \omega_k \hat{b}_k^\dagger \hat{b}_k \quad (2)$$

where $\Delta = \omega_{eg} - \omega$ is the detuning. Now we use the transformation [10, 15]

$$\hat{T} = \prod_k e^{\hat{\sigma}_{ee} \frac{\lambda_k}{\omega_k} (\hat{b}_k^\dagger - \hat{b}_k)} \quad (3)$$

to obtain the Hamiltonian $\hat{\mathcal{H}}_T = \hat{T} \hat{\mathcal{H}} \hat{T}^\dagger$

$$\begin{aligned} \hat{\mathcal{H}}_T = & (\Delta - \Delta_\eta) \hat{\sigma}_{ee} + \sum_k \omega_k \hat{b}_k^\dagger \hat{b}_k \\ & + g \left[\hat{a}^\dagger \hat{\sigma}_- \prod_k \hat{D}_{\hat{b}}(\eta_k) + \hat{\sigma}_+ \hat{a} \prod_k \hat{D}_{\hat{b}}^\dagger(\eta_k) \right], \end{aligned} \quad (4)$$

with $\eta_k = \lambda_k / \omega_k$, $\Delta_\eta = \sum_k \omega_k \eta_k^2$ is the so-called polaron shift [15] and $\hat{D}_{\hat{b}}(\eta_k) = \exp(\eta_k \hat{b}^\dagger - \eta_k^* \hat{b})$. For simplicity we look at the case $\Delta = \Delta_\eta$ to obtain

$$\hat{\mathcal{H}}_T = g \left[\hat{a}^\dagger \hat{\sigma}_- \prod_k \hat{D}_{\hat{b}}(\eta_k) + \hat{\sigma}_+ \hat{a} \prod_k \hat{D}_{\hat{b}}^\dagger(\eta_k) \right] + \sum_k \omega_k \hat{b}_k^\dagger \hat{b}_k. \quad (5)$$

Now by transforming to an interaction picture

$$\hat{H}_I = g \left[\hat{a}^\dagger \hat{\sigma}_- \prod_k \hat{D}_{\hat{b}}(\eta_k e^{-i\omega_k t}) + \hat{\sigma}_+ \hat{a} \prod_k \hat{D}_{\hat{b}}^\dagger(\eta_k e^{-i\omega_k t}) \right] \quad (6)$$

and applying the rotating wave approximation in the above equation, the final Hamiltonian is obtained:

$$\hat{H}_{rwa} = \tilde{g} \left[\hat{a}^\dagger \hat{\sigma}_- \prod_k L_{\hat{n}_k}(-\eta_k^2) + \hat{\sigma}_+ \hat{a} \prod_k L_{\hat{n}_k}(-\eta_k^2) \right] \quad (7)$$

where $L_{\hat{n}_k}$ are the Laguerre polynomials of order \hat{n}_k [16, 17] and $\tilde{g} = g \exp(\xi/2) \equiv g \exp(-\sum_k \eta_k^2/2)$ is a rescaled Rabi vacuum frequency. The parameter ξ is sometimes referred to as the Huang-Rhys factor [18], and it is usually very small, $\xi \ll 1$, [19, 20] but it can become much larger, $\xi \sim 1$, [21]. The above equation is readily solvable, finding the evolution operator as

$$\hat{U} = \hat{U}_{ee} \hat{\sigma}_{ee} + \hat{U}_{gg} \hat{\sigma}_{gg} + \hat{U}_{eg} \hat{\sigma}_- + \hat{U}_{ge} \hat{\sigma}_+, \quad (8)$$

where

$$\hat{U}_{ee}(t; \hat{n}) = \cos \hat{\Omega}_{k, \hat{n}+1} t, \quad (9)$$

$$\hat{U}_{ge}(t; \hat{n}) = -i\epsilon \hat{a} \frac{\sin \hat{\Omega}_{k, \hat{n}} t}{\hat{\Omega}_{k, \hat{n}}}, \quad (10)$$

$$\hat{U}_{eg}(t; \hat{n}) = -i\epsilon \hat{a}^\dagger \frac{\sin \hat{\Omega}_{k, \hat{n}+1} t}{\hat{\Omega}_{k, \hat{n}+1}}, \quad (11)$$

and

$$\hat{U}_{gg}(t; \hat{n}) = \cos \hat{\Omega}_{k, \hat{n}} t, \quad (12)$$

with

$$\hat{\Omega}_{\hat{n}} = \hat{\epsilon} \sqrt{\hat{n}} = \tilde{g} L_{\hat{n}_k}(-\eta_k^2) \sqrt{\hat{n}}. \quad (13)$$

III. DYNAMICS

Having the evolution operator, we can in principle calculate any properties we want, in particular we look at the Rabi oscillations for the two-levels system, which has been studied experimentally in quantum dot systems [20]. By means of the inversion operator $\hat{\sigma}_z = |e\rangle\langle e| - |g\rangle\langle g|$

$$W(t) = \text{Tr}\{\rho(t)\hat{\sigma}_z\} \quad (14)$$

where $\rho(t) = \hat{U}\rho(0)\hat{U}^\dagger$ and $\rho(0)$ is the initial density matrix, Rabi oscillations will be analyzed. This initial state is chosen as the fully separable state

$$\rho(0) = \prod_k \rho_k(0) |0, e\rangle\langle 0, e| \quad (15)$$

with the atom excited, the cavity mode in vacuum and the phonon modes are all assumed to be in a thermal distribution

$$\rho_k(0) \sum_{n_k=0}^{\infty} |c_{n_k}|^2 |n_k\rangle\langle n_k| = \sum_{n_k=0}^{\infty} \frac{\bar{n}_k^{n_k}}{(\bar{n}_k + 1)^{n_k+1}} |n_k\rangle\langle n_k|. \quad (16)$$

The inversion can be written explicitly as

$$W(t) = \sum_{\{n_k\}} \prod_k |c_{n_k}|^2 \cos \left(2\tilde{g} \prod_{k'} L_{n_{k'}}(-\eta_{k'}^2) t \right), \quad (17)$$

where the summation goes from 0 to ∞ and runs over all modes. For $t = 0$ we have $W(0) = 1$ as expected, while for $t \neq 0$ the sum will in general differ from 1. Interestingly we note that at zero temperature, $T = 0$, $|c_{n_k}| = \delta_{n_k, 0}$ for all k and thus, at absolute zero temperature the system Rabi oscillations are intact in amplitude but with a rescaled frequency [12]. Because the argument of the cosine function consists of a product of functions with different mode indices k , the expression can in general not be separated. Nonetheless, under some assumptions the inversion (17) can be greatly simplified. As mentioned in the previous section, usually $\eta \ll 1$ and we may expand the Laguerre polynomials

$$L_n(-\eta^2) = \sum_{m=0}^n \binom{n}{m} \frac{\eta^{2m}}{m!} = 1 + n\eta^2 + \frac{n(n-1)}{4} \eta^4 + \dots \quad (18)$$

Keeping only zeroth and first order terms in η_k^2 , the inversion can be written, after some algebra, as

$$\begin{aligned} W(t) = & \cos(2\tilde{g}t) \mathcal{R}e \left(\prod_k \frac{1}{\bar{n}_k + 1 - \bar{n}_k e^{i2\tilde{g}t\eta_k^2}} \right) \\ & - \sin(2\tilde{g}t) \mathcal{I}m \left(\prod_k \frac{1}{\bar{n}_k + 1 - \bar{n}_k e^{i2\tilde{g}t\eta_k^2}} \right). \end{aligned} \quad (19)$$

In the following we use dimensionless variables such that the quantum dot-cavity coupling $g = 1$, but keep it in the formulas for clarity. There are some special cases worth studying separately.

A. Single phonon mode

In the simplest case consisting of a single phonon mode characterized by η and \bar{n} , the inversion (19) simplifies to

$$W(t) = \frac{(\bar{n} + 1) \cos(2\tilde{g}t) - \bar{n} \cos[2\tilde{g}t(1 + \eta^2)]}{(\bar{n} + 1)^2 + \bar{n}^2 - 2\bar{n}(\bar{n} + 1) \cos(2\tilde{g}t\eta^2)}. \quad (20)$$

The second term oscillates with a slightly shifted frequency causing a collapse of the inversion. When the two competing terms return back in phase, at times

$$t_{rev}^{(1)} = k \frac{\pi}{\tilde{g}\eta^2}, \quad k = 1, 2, 3, \dots, \quad (21)$$

inversion revivals occur. These are perfect within the small η^2 expansion. For short times t , the inversion may be further approximated to give

$$W(t) = \frac{\cos(2\tilde{g}t)}{1 + 8\bar{n}(\bar{n} + 1)\tilde{g}^2\eta^4t^2}, \quad 2\tilde{g}t\eta^2 \ll 1, \quad (22)$$

and we conclude that the envelope function, determining the collapse time, is a Lorentzian with width

$$t_{col}^{(1)} = \frac{1}{\sqrt{8\bar{n}(\bar{n} + 1)}\tilde{g}\eta^2}. \quad (23)$$

For larger values of η^2 , higher order terms in the expansion (18) must be included and perfect revivals are no longer present. Additionally, it is likely that the rotating wave approximation applied in eq. (6) breaks down for increasing η^2 . In fig. 1 we display three different examples of the atomic inversion (17), and hence calculated from the RWA formula where the small η expansion has not been applied. The upper plot has a large average number of phonons; $\bar{n} = 40$, and $\eta = 0.1$ and it is clear that perfect revivals are lost due to large η . In the second plot the number of phonons are the same but $\eta = 0.02$ and the revivals are almost perfect. Note as well that the revival times are longer in this example. Finally in the last plot $\bar{n} = 2$ and $\eta = 0.01$ and we can conclude that a lower temperature of the reservoir increases the collapse time. These observations are in perfect agreement with the above derived approximations, and for figs. 1 (b) and (c) the expression (20) almost exactly agrees with the exact one. In the long time evolution of the system, the higher order terms of the Laguerre expansion (18) start to play an important role, and *fractional* and *super* revivals may occur [22].

B. N identical phonon modes

By studying several identical phonon modes one may see the effect of multi modes in a simple analytic way. For N identical modes ($\eta_k = \eta_{k'} |c_{n_k}| = |c_{n_{k'}}|$ for $n_k = n_{k'}$)

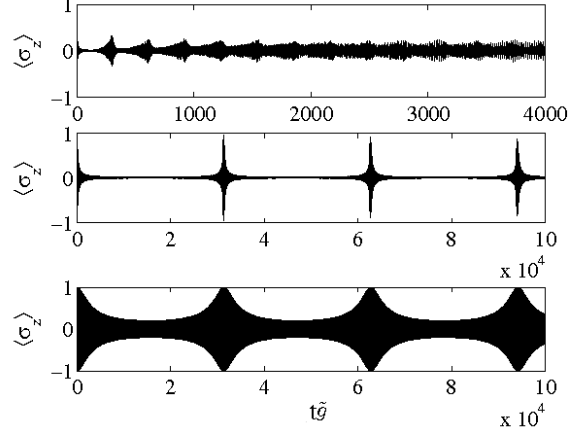


FIG. 1: The atomic inversion $W(t)$ as a function of time t for the single mode bath. The dimensionless parameters are $\eta = 0.1$ and $\bar{n} = 40$ for the upper plot, $\eta = 0.01$ and $\bar{n} = 40$ for the middle plot and $\eta = 0.01$ and $\bar{n} = 2$ for the lower plot.

of the phonon bath, the inversion (19) becomes

$$W(t) = \left[\frac{1}{(\bar{n} + 1)^2 + \bar{n}^2 - 2\bar{n}(\bar{n} + 1) \cos(2\tilde{g}t\eta^2)} \right]^N \times \sum_{j=0}^N \left\{ \binom{N}{j} (-\bar{n})^{N-j} (\bar{n} + 1)^j \times \cos[2\tilde{g}t(1 + (N-j)\eta^2)] \right\}. \quad (24)$$

Now the inversion is built up of several competing terms and the collapse will be more pronounced. This also follows directly from noting that the envelope function in this case is an identical Lorentzian as for the situation with a single mode, except that is is taken to the N th power. The collapse time can therefore be approximated by

$$t_{col}^{(N)} = \frac{(\sqrt[N]{2} - 1)^{1/2}}{\sqrt{8\bar{n}(\bar{n} + 1)}\tilde{g}\eta^2}. \quad (25)$$

Fractional revivals, hardly visible, take place at

$$t_{j,rev}^{(N)} = k \frac{\pi}{(N-j)\tilde{g}\eta^2}, \quad k = 1, 2, 3, \dots, \quad (26)$$

and for the perfect revivals we have $t_{rev}^{(N)} = t_{rev}^{(1)}$. Figure 2 shows the atomic inversion for different number of identical modes obtained from eq. (24) in (a) and from eq. (17) in (b). We note that the approximation breaks down when the number of phonon modes is increased; the revivals are no longer perfect and they occur earlier. The fact that the revival times are shorter is due to the higher order terms in the expansion (18), which becomes

more important for a large number of modes. Note, however, that η^2 is rather large in this example in order to see the effect.

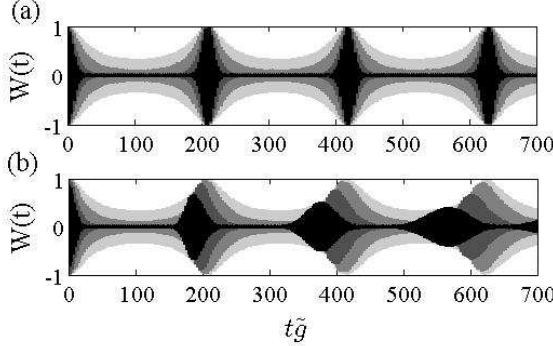


FIG. 2: The atomic inversion for 10 (black), 5 (dark gray), 2 (gray) and 1 (light gray) identical phonon modes. The upper plot (a) displays the results using the small η^2 expansion (24), and the lower (b) shows the exact (17). The parameters are $\bar{n} = 1$ and $\eta^2 = 0.015$.

C. N different phonon modes

In a more realistic model the phonon bath consists of non-identical modes, and depending on the model studied one has different spectral functions $J(\omega) = \sum_k \lambda_k^2 \delta(\omega - \omega_k)$ [23]. For the frequencies of interest here, $J(\omega)$ has a simple power law behaviour [24], resulting in a

$$\eta_k^2 = \kappa \omega_k^s, \quad s = \dots, -2, -1, 0, 1, 2, \dots, \quad (27)$$

where κ is a constant. The power s depends on matter properties, for example; *ohmic damping* $J(\omega) \propto \omega$, *phonon damping* $J(\omega) \propto \omega^3$ or *impurity damping* $J(\omega) \propto \omega^5$, but it also depends on system dimensions. We take $\omega_k = \omega_0 k$, $k = 1, 2, 3, \dots$ such that ω_0 determines the frequency spacing, while the thermal phonon distributions are determined from the average phonon numbers

$$\bar{n}_k = \left[\exp \left(\frac{\omega_k}{\tilde{T}} \right) - 1 \right]^{-1}, \quad (28)$$

for some scaled temperature \tilde{T} . Often a frequency “cut-off” is introduced for the spectral function, but because the vacuum modes do not affect the system dynamics in our case such a cut-off is not needed. Defining $c_k = 8\bar{n}_k(\bar{n}_k + 1)\tilde{g}^2\eta_k^4$, and using the same arguments as above the collapse time in the small η^2 expansion is given by

$$\prod_k (1 + c_k t_{col}^2) = 2. \quad (29)$$

By further introducing

$$\begin{aligned} r_k &= \sqrt{(\bar{n}_k + 1)^2 + \bar{n}_k^2 - 2\bar{n}_k(\bar{n}_k + 1)\cos(2\tilde{g}t\eta_k^2)}, \\ \theta_k &= -\arctan \left[\frac{\bar{n}_k \sin(2\tilde{g}t\eta_k^2)}{\bar{n}_k + 1 - \bar{n}_k \cos(2\tilde{g}t\eta_k^2)} \right] \end{aligned} \quad (30)$$

the approximated atomic inversion (19) can be written as

$$W(t) = \frac{\cos(2\tilde{g}t + \theta)}{r}, \quad (31)$$

where $\theta = \sum_k \theta_k$ and $r = \prod_k r_k$. In fig. 3, five examples of the atomic inversion in the small η^2 expansion are displayed for different powers s . Perfect revivals clearly occur for the $s = 0, s = 1$ and $s = 2$ cases, while for $s = -2$ and $s = -1$ the revivals are never fully perfect even at long times. This is because if $s = 0, 1, 2, \dots$ we have $\eta_k^2 = \kappa \omega_k^s = \kappa \omega_0^s k^s \equiv \eta_0^2 j$ where j is a positive integer, which does not hold if $s = \dots, -2, -1$. Note that the revivals are a consequence of the non Markovian treatment of the problem.

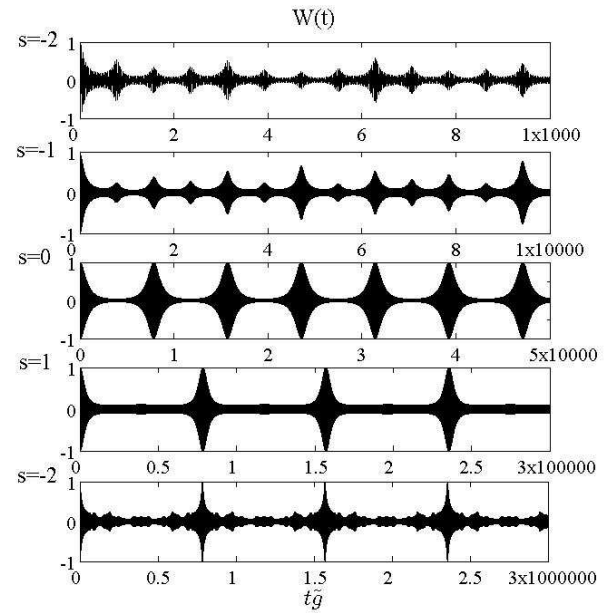


FIG. 3: Atomic inversion for different phonon modes obtained from the small η^2 expansion (19). The plots show respectively from top to bottom the cases with powers $s = -2, -1, 0, 1, 2$ of eq. (27). The other parameters are the same for all five cases; $T = 0.2$, $\kappa = 0.0004$ and $\omega_0 = 0.1$.

IV. BEYOND THE ROTATING WAVE APPROXIMATION

So far all the results have been derived or calculated within the RWA, which for $g\eta/\omega \ll 1$ is expected to be justified. In this section we calculate the atomic inversion

by numerically diagonalize the truncated Hamiltonian of eq. (5). The size of the Hamiltonian is chosen such that convergence of its eigenstates is guaranteed. We restrict the analysis to the one phonon mode case (apart from the example of fig. 8), which already explains most effects. In the Fock state basis $\{|m\rangle\}$ of the phonon mode, the matrix elements of the Hamiltonian are obtained by using the formula

$$D_{mn} \equiv \langle m | \hat{D}(\eta) | n \rangle e^{-\eta^2/2} \eta^{n-m} \sqrt{\frac{m!}{n!}} L_m^{n-m}(\eta^2), \quad m \leq n, \quad (32)$$

where L_i^j is an associated Laguerre polynomial, and we have $D_{mn} = (-1)^{n-m} D_{nm}$. As already mentioned, the RWA relies on the ratios $g\eta_k/\omega_k$ and we will analyze the effects of a changing ω_k , while η_k is kept fixed.

For lowest order truncation of the Hamiltonian, one keeps only a single Fock state of the phonon mode, and the results above where the RWA has been imposed are regained [25]. In this approximation, when the initial states of the phonon modes are on the form $|c_{n_k}\rangle = \delta_{n_k, n'_k}$, the combined quantum dot-cavity system persists perfect Rabi oscillations with a rescaled vacuum Rabi frequency $g \rightarrow \tilde{g} \prod_{n'_k} L_{n'_k}(-\eta_{n_k}^2)$. For zero temperature, all the modes are in the vacuum and the above approximation simply gives a rescaled frequency $g \rightarrow \tilde{g}$, which is the result presented in [12]. To go beyond the RWA one needs to include more terms/matrix elements in the Hamiltonian arising from the phonon bath. For Fock states $n > 0$ the single state truncation is even more likely to break down, which is seen by expanding the elements of (32) for small η

$$\langle m | \hat{D}(\eta) | m \rangle \approx e^{-\eta^2/2} [1 - m\eta^2]. \quad (33)$$

$$\langle m - 1 | \hat{D}(\eta) | m \rangle \approx e^{-\eta^2/2} \eta [1 - \sqrt{m}(m + 1)\eta^2].$$

Thus, for increasing temperature, or equivalently \bar{n} , the off diagonal terms of (32) become more important. However, also at zero temperature the RWA breaks down if the phonon frequency ω becomes sufficiently small, and interesting new features appear.

In fig. 4 we display the atomic inversion as a function of time $t\tilde{g}$ and frequency ω for the zero temperature case. For $\omega = \omega_c = 20\eta$ and at times $t_c \approx 15 + 30j$, and $j = 0, 1, 2, 3, \dots$ a new bright peak occur. The same holds for any Fock state and therefore also for any initial state of the phonon mode. The structure of fig. 4 is well known in many fields of physics and is often referred to as *dislocation* [26]. For example, in BECs [27], in classical optics [28] and in crystals [29]. The interference between waves with vortices (singularities) gives rise to a phase processing non analytic behavior at the critical points. In our case, the phases may be obtained from fourier transforming the inversion $W(t)$. In fig. 5 we display the fourier transformed atomic inversion $\tilde{W}(\varpi)$ as a function of the scaled phonon frequency ω/η . We only show the positive part $\varpi > 0$ since the negative part is identical

but reflected. From the figure one notes a discontinuity at the critical point ω_c .

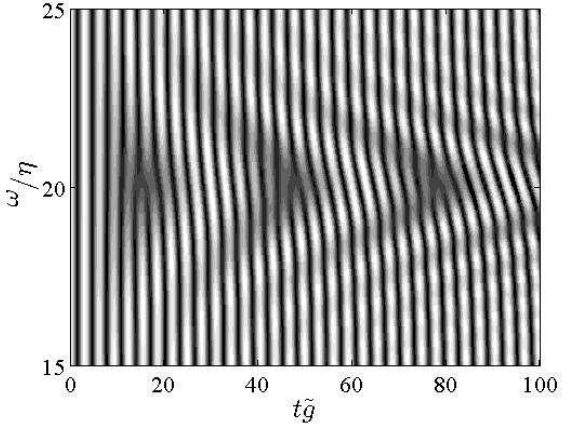


FIG. 4: Contour plot of the atomic inversion as function of scaled time and scaled phonon frequency. The critical points were an extra “fringe” occur are due to discontinuities in the Rabi frequency. Here $\eta = 0.1$ and $\bar{n} = 0$.

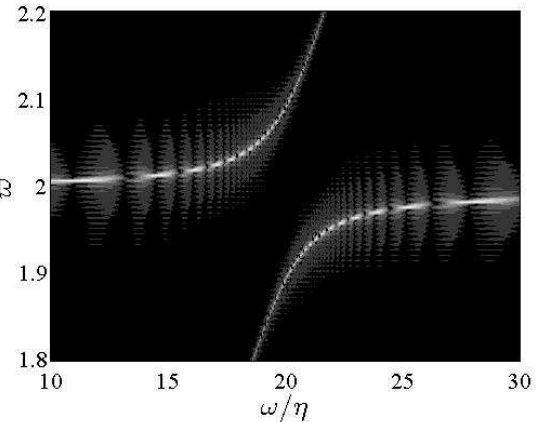


FIG. 5: The fourier transformed atomic inversion of fig. 4. At the critical point ω_c the frequency becomes discontinuous.

Figures 4 and 5 are calculated using a size of the truncated Hamiltonian such that convergence is assured, but interestingly, including only first order corrections to the RWA (adding a non-zero $\langle 0 | \hat{D}(\eta) | 1 \rangle$) the same dislocation pattern is obtained. In this case the Hamiltonian,

for an initial vacuum phonon mode, becomes

$$H_{vac} = \begin{bmatrix} -\frac{\omega}{2} & 0 & D_{00} & D_{01} \\ 0 & \frac{\omega}{2} & -D_{01} & D_{11} \\ D_{00} & -D_{01} & -\frac{\omega}{2} & 0 \\ D_{01} & D_{11} & 0 & \frac{\omega}{2} \end{bmatrix}, \quad (34)$$

with eigenvalues

$$\begin{aligned} \lambda_{\pm} &= \frac{D_{00} - D_{11}}{2} \pm \frac{1}{2} \sqrt{[\omega - (D_{00} + D_{11})]^2 + 4D_{01}^2} \\ \mu_{\pm} &= \frac{D_{00} + D_{11}}{2} \pm \frac{1}{2} \sqrt{[\omega + (D_{00} + D_{11})]^2 + 4D_{01}^2}. \end{aligned} \quad (35)$$

These eigenvalues are shown in fig. 6; λ_{\pm} (solid lines) and μ_{\pm} (dashed lines). The two λ_{\pm} eigenvalues indicate an avoided level crossing, which is due to the non-zero matrix element D_{01} . The gap of the avoided crossing (energy difference) is in lowest order given by $\Delta E = 2D_{01}$. Note that there is another level crossing between the λ_- and the μ_- energies for lower ω , which is not avoided. Including more terms in the Hamiltonian would lead to that this would also become an avoided crossing, but with a much smaller gap since it would be of “higher order” (described by a multi step process). In general, increasing the size of the Hamiltonian will give several avoided level crossing, but still there is only one of first order, and it will dominate the dynamics, which explains why the dislocation pattern of fig. 4 is obtained also in this first order correction. The avoided crossing occurs at

$$\omega_c = D_{00} + D_{11} = e^{-\eta^2/2}(2 + \eta^2), \quad (36)$$

where λ_{\pm} have extreme points, and their corresponding values at these points are $\lambda_{\pm}(\omega_c) = (1 \pm \frac{\eta}{2})\eta \exp(-\eta^2/2)$. The critical times are then given by

$$t_c = \frac{\pi e^{\eta^2/2}}{\eta} \left(j + \frac{1}{2} \right), \quad j = 0, 1, 2, \dots \quad (37)$$

Note that starting from any initial Fock state $|n\rangle$ of the phonon mode will give the same critical frequency ω_c , while the gap will differ slightly. Thus, for a more general initial state of the phonon mode, the slight energy differences between the eigenenergies cause interference of competing terms and there will be regions of no Rabi oscillations, while the critical points will be approximately at the same locations. Figure 7 is showing the same as in fig. 4 but for an initial thermal state with $\bar{n} = 3$.

To see the effect of multi phonon modes we include a second mode with twice the frequency, $\omega_2 = 2\omega_1$ and $\eta_2 = \eta_1/2$. Again only the first order corrections to the

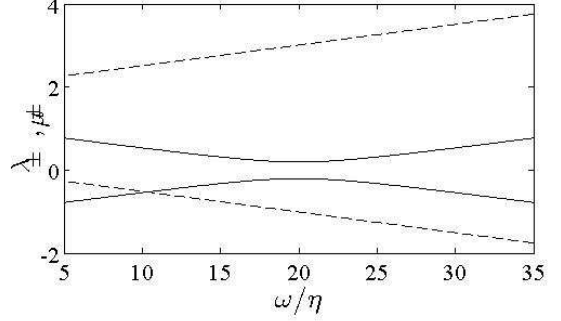


FIG. 6: The eigenenergies (35) of the 4×4 Hamiltonian (34). Solid lines are the λ_{\pm} energies and dashed lines the μ_{\pm} . The λ_{\pm} energies exhibit a level crossing which is avoided due to the non vanishing D_{01} -term.

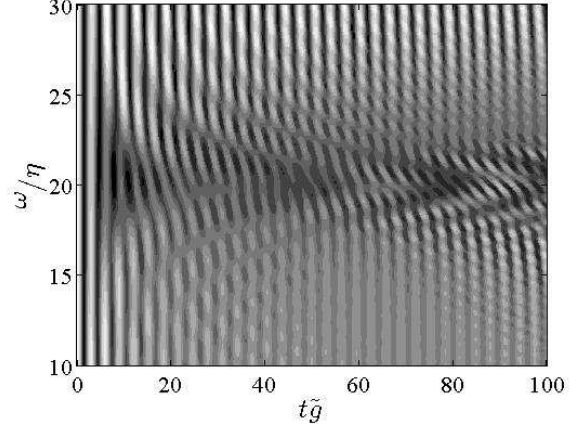


FIG. 7: The same as in fig. 4 but for an initial thermal state with $\bar{n} = 3$. The “dislocation-points” are located at the same places as in fig. 4. However, the different eigenenergies interfere giving the wavy pattern of the inversion.

RWA Hamiltonian is taken into account, which, according to the above discussion, should give the general structure of the dynamics. The eight energy eigenvalues are displayed in fig. 8. The critical frequency $\omega_c^{(1)}$ for the avoided crossings corresponding to the one mode case is the same. However, a new “set” of lowest order avoided crossings occur at $\omega_c^{(2)} = \omega_c^{(1)}/2$. Since the gap scales as η , the higher frequency critical points will affect the dynamics less.

We conclude this section by shortly investigating the long time behaviour of the inversion without the RWA. Figure 9 gives two examples of the atomic inversion in the one phonon mode case. The black curves corresponds to a very large frequency ω such that it coincides with the

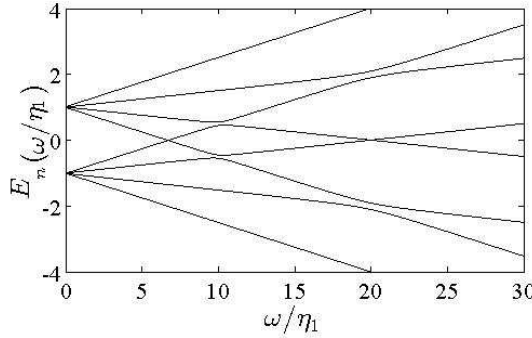


FIG. 8: The eigenenergies corresponding to the two phonon mode model with first order corrections to the RWA situation. We have $\eta_1 = 2\eta_2 = 0.01$ and $\omega \equiv \omega_1 = \omega_2/2$. Now there are two sets of critical frequencies; $\omega_c^{(2)} \approx 10$ and $\omega_c^{(1)} \approx 20$.

RWA result (this has been numerically checked), while gray and light gray curves show how the inversion deviates from the RWA results when the frequency is decreased. Figure 10 shows the dependence of the phonon frequency on the inversion, (a) gives the large ω case and (b) the small ω situation. The frequency $\omega \approx 63\eta$ corresponds to the critical frequency ω_c around which the revival pattern breaks down. Then there is a line at $\omega \approx 92\eta$ where the collapse time goes to infinity and the revivals cease to exist. For such ω the spectrum has a particular structure; the eigenvalues come in “identical” equally distant pairs, therefore there are only two relevant frequencies; one related to the energy difference between pairs and one related to the energy difference within each pair. In the simplified model corresponding to a 4×4 Hamiltonian of fig. 6, this occurs for an ω such that there are only two different energy differences instead of the general case of three. This means that $\lambda_+ - \lambda_- = \lambda_- - \mu_-$ and by neglecting D_{01} one finds $\omega \approx \exp(-\eta^2/2)(3 + \eta^2)$, which for the above example gives $\omega \approx 94\eta$ in good agreement with the figure. Note also that the asymptotic revival times for large and small ω differ by approximately a factor of 2.

V. CONCLUSIONS

We have studied a quantum dot strongly coupled to a single high-finesse optical cavity mode by applying methods usually applied in ion-laser interactions, namely the decomposition of the Glauber displacement operator in Laguerre polynomials. This allowed us to obtain results for many phonon modes beyond the Born-Markov approximation. We have studied several cases, including N identical and N different phonon modes, i.e. the case of non-zero temperature. Analytical expressions for the

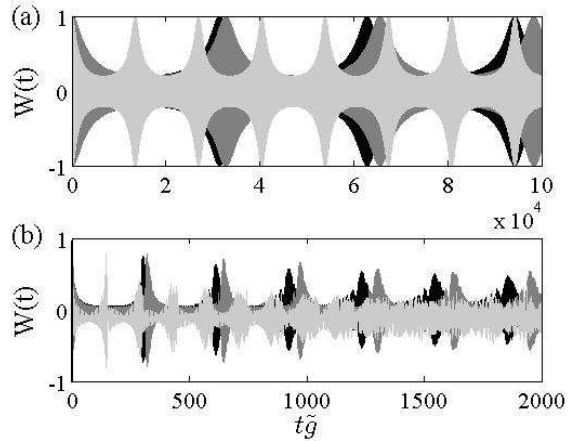


FIG. 9: Atomic inversion obtained numerically from the exact Hamiltonian (5). In the upper plot (a), the average number of photons is $\bar{n} = 2$ and $\eta = 0.01$, while in (b) $\bar{n} = 10$ and $\eta = 0.1$. In (a) we have $\omega = 10000\eta$ (black), $\omega = 1000\eta$ (gray) and $\omega = 100\eta$ (light gray) and for (b) $\omega = 1000\eta$ (black), $\omega = 100\eta$ (gray) and $\omega = 10\eta$ (light gray). The black curves are almost identical to the ones given by the Hamiltonian when the RWA has been imposed.

collapse and revival times of the Rabi oscillations have been derived analytically, valid in a large range of parameters. We have also obtained new results for the non RWA regime. Among these, the most interesting ones are; the absence of collapse-revivals due to an equidistant spectrum and dislocation-like behaviors of the Rabi oscillations arising from avoided level crossings of the spectrum. Recently, [30], it was shown that the current model studied in this paper exhibits a phase transition when coupled to an ohmic phonon reservoir. For certain parameters, especially of the ratio of QD-cavity coupling and QD-bath coupling, the decay of Rabi oscillations vanishes. Using the approach presented here to analyze such a phase transition is planned for the future.

Acknowledgments

This work was supported by EU-IP Programme SCALA (Contract No. 015714), the Swedish Government/Vetenskapsrådet and Consejo Nacional de Ciencia y Tecnología.

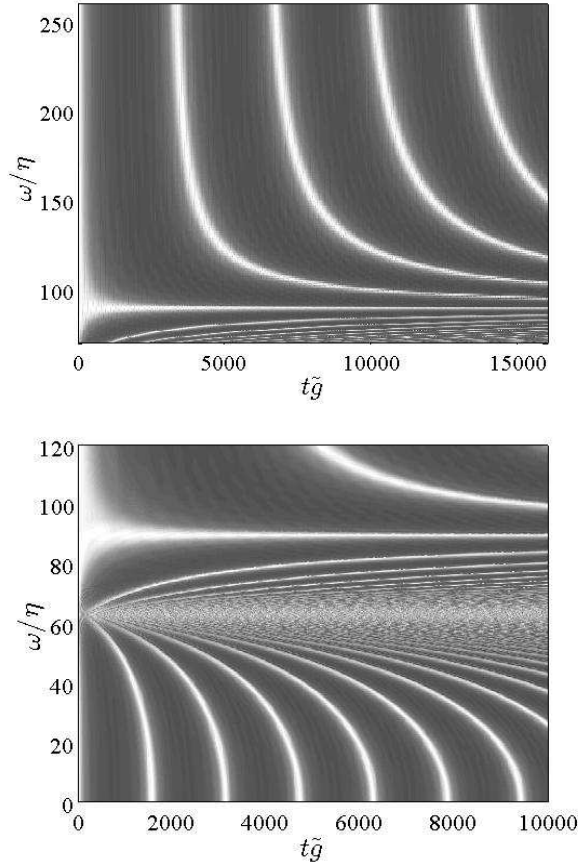


FIG. 10: Large time atomic inversion as function of time and phonon frequency. The critical frequency, at the avoided level crossing, is $\omega_c = \exp(-\eta^2/2)(2 + \eta^2) \approx 63\eta$. At $\omega = \exp(-\eta^2/2)(3 + \eta^2) \approx 92\eta$ the collapse time goes to infinity. Here $\eta^2 = 0.001$ and $\bar{n} = 3$.

[1] A. Imamoglu, D. D. Awschalom, G. Burkard, D. P. Di Vincenzo, D. Loss, M. Sherwin, and A. Small, Phys. Rev. Lett. **83**, 4204 (1999); A. Miranowicz, . K. zdemir1, Y. Liu, Masato Koashi, N. Imoto1, and Y. Hirayama1, Phys. Rev. A **65**, 062321 (2002); M. Feng, I. D'Amico, P. Zanardi, and F. Rossi, Phys. Rev. A **67**, 014306 (2003); X. Wang, M. Feng and B.C. Sanders, Phys. Rev. A **67**, 022302 (2003).

[2] J. M. Gérard, B. Sermage, B. Gayral, B. Legrand, E. Costard, and V. Thierry-Mieg, Phys. Rev. Lett. **81**, 1110 (1998); C. Becher1, A. Kiraz1, P. Michler1, A. Imamolu1, W. V. Schoenfeld, P. M. Petroff, Lidong Zhang, and E. Hu, Phys. Rev. B **63**, 121312 (2001); A. Kiraz, C. Reese, B. Gayral, L. Zhang, W.V. Schoenfeld, B.D. Gerardot, P.M. Petroff, E.L. Hu, and A. Imamoglu, J. Opt. B **5**, 129 (2003).

[3] B.W. Shore and P.L. Knight, J. Mod. Optics **40** 1195 (1993).

[4] M. Brune, S. Haroche, J. M. Raimond, L. Davidovich, and N. Zagary, Phys. Rev. A **45**, 5193 (1992); M. Brune, E. Hagley, J. Dreyer, X. Maitre, A. Maali, C. Wunderlich, J. M. Raimond, and S. Haroche, Phys. Rev. Lett. **77**, 4887 (1996); S. Brattke, B. T. H. Varcoe, and H. Walther, Phys. Rev. Lett. **86**, 3534 (2001).

[5] J. M. Raimond, M. Brune, and S. Haroche, Rev. Mod. Phys. **73**, 565 (2001).

[6] D. Leibfried, R. Blatt, C. Monroe, and D. Wineland, Rev. Mod. Phys. **75**, 281 (2003).

[7] D. Kielpinski, C. Monroe, and D. J. Wineland, Nature **417**, 709 (2002).

[8] D. Leibfried, D. M. Meekhof, C. Monroe, B. E. King, W. M. Itano, and D. J. Wineland, J. Mod Opt. **44**, 2485 (1997); C. Roos, T. Zeiger, H. Rohde, H. C. Nagerl, J. Eschner, D. Leibfried, F. Schmidt-Kaler, and R. Blatt,

Phys. Rev. Lett. **83**, 4713 (1999).

[9] A. Wallraff, D. I. Schuster, A. Blais, L. Frunzio, R. S. Huang, J. Majer, S. Kumar, S. M. Girvin, R. J. Schoelkopf, Nature **431**, 162 (2004); D. I. Schuster, A. A. Houck, J. A. Schreier, A. Wallraff, J. M. Gambetta, A. Blais, L. Frunzio, J. Majer, B. Johnson, M. H. Devoret, S. M. Girvin, R. J. Schoelkopf, Nature **445**, 515 (2007); K. Hennessy, A. Badolato, M. Winger, D. Gerace, M. Atatüre, S. Gulde, S. Fält, E. L. Hu, and A. Imamoglu, Nature **445**, 896 (2007).

[10] A. Wuergler, Phys. Rev. B **57**, 347 (1998).

[11] I. Wilson-Rae and A. Imamoglu, Phys. Rev. B **65**, 235311 (2002).

[12] L. Wai-Sang, and Z. Ka-Di, Chin. Phys. Lett. **20**, 1568 (2003); Z. Ka-Da, and L. Wai-Sang, Phys. Lett. A **314**, 380 (2003).

[13] H. -P. Breuer, and F. Petruccione, *The theory of open quantum systems*, (Oxford University Press, 2003); C. W. Gardiner, and P. Zoller, *Quantum Noise*, (Springer Verlag, 2004).

[14] Ka-Di Chin, Z-J. Wu, X-Z. Yuan, and H. Zheng, Phys. Rev. B **71**, 235312 (2005).

[15] C.B. Duke and G.D. Mahan, Phys. Rev. **139**, A1965 (1965).

[16] D. Leibfried, R. Blatt, C. Monroe, and D. Wineland, Reviews of Modern Physics **75**, 281 (2003).

[17] S. Wallentowitz, W. Vogel and P.L. Knight, Phys. Rev. A **59** 531 (1999); S. Wallentowitz adn W. Vogel, Phys. Rev. A **58** 679 (1998).

[18] K. Huang, and A. Rhys, Proc. R. Soc. Lond. A **204**, 406 (1950).

[19] R. Heitz, I. Mukhametzhanov, O. Stier, A. Madhukar, and D. Bimberg, Phys. Rev. Lett. **83**, 4654 (1999)

[20] T. H. Stievater, X. Li1, D. G. Steel, D. Gammon, D. S. Katzer, D. Park, C. Piermarocchi, and L. J. Sham, Phys. Rev. Lett. **87**, 133603 (2001); H. Kamada, H. Gotoh, J. Temmyo, T. Takagahara, and H. Ando, Phys. Rev. Lett. **87**, 246401 (2001).

[21] V. Turck, S. Rodt, O. Stier, R. Heitz, R. Engelhardt, U. W. Pohl, D. Bimberg, and R. Steingruber, Phys. Rev. B **61**, 9944 (2000).

[22] M. V. Satyanarayana, P. Rice, R. Vyas, and H. J. Carmichel, J. Opt. Soc. Am. B **6**, 228 (1989); S. S. Averbukh, Phys. Rev. A **46**, R2205 (1992); P. F. Gra, and C. Jedrzejek, Phys. Rev. A **48**, 3291 (1993).

[23] G. D. Mahan, *Many-Particle Physics*, (Kluwer, new York 2000).

[24] A. J. Leggett, S. Chakravarty, A. T. Dorsey, M. P. A. Fisher, A. Garg, and W. Zwerger, Rev. Mod. Phys. **59**, 1 (1987).

[25] J. Larson, and H. Moya-Cessa, math-ph/0611067, accepted in J. Mod. Opt.

[26] D. Hull, and D. J. Bacon, *Introduction to Dislocations*, (Butterworth-Heinemann, 2001); J. Weertman, and J. R. Weertman, *Elementary Dislocation Theory*, (Oxford University Press, 2006).

[27] J. Tempere, and J. T. Devreese, Solid State Comm. **108**, 993 (1998); S. Stock, Z. Hadzibabic, B. Battelier, M. Cheneau, and J. Dalibard, Phys. Rev. Lett. **95**, 190403 (2005).

[28] L. Allen, M. J. Padgett, and M. Babiker, Prog. Opt. **39**, 291 (1999); J. Leach, M. R. Dennis, J. Courtial, and M. J. Padgett, Nature **432**, 165 (2004).

[29] W. T. Read, and W. Shockley, Phys. Rev. **78**, 275 (1959); A. Carpio, and L. L. Bonilla, Phys. Rev. B **71**, 134105 (2005).

[30] C. Q. Wu, J. X. Li, D. H. Lee, cond-mat/0703238.